Pectin-coated boron nitride nanotubes: *In vitro* cyto-/immune-Compatibility on RAW 264.7 macrophages

Antonella Rocca, Attilio Marino, Serena Del Turco, Valentina Cappello, Paola Parlanti, Mario Pellegrino, Dmitri Golberg, Virgilio Mattoli, Gianni Ciofani

PII: S0304-4165(16)30006-X
DOI: doi: 10.1016/j.bbagen.2016.01.020
Reference: BBAGEN 28378

To appear in: *BBA - General Subjects*

Received date: 17 November 2015
Revised date: 11 January 2016
Accepted date: 24 January 2016

Please cite this article as: Antonella Rocca, Attilio Marino, Serena Del Turco, Valentina Cappello, Paola Parlanti, Mario Pellegrino, Dmitri Golberg, Virgilio Mattoli, Gianni Ciofani, Pectin-coated boron nitride nanotubes: *In vitro* cyto-/immune-Compatibility on RAW 264.7 macrophages, *BBA - General Subjects* (2016), doi: 10.1016/j.bbagen.2016.01.020

Pectin-Coated Boron Nitride Nanotubes: *In vitro* Cyto- / Immune-Compatibility on RAW 264.7 Macrophages

Antonella Rocca[a,b]*, Attilio Marino[a,b], Serena Del Turco[c], Valentina Cappello[d], Paola Parlanti[d,e], Mario Pellegrino[f], Dmitri Golberg[g], Virgilio Mattoli[b], Gianni Ciofani[b,h]*

[a] Scuola Superiore Sant'Anna, The BioRobotics Institute, Viale Rinaldo Piaggio 34, 56025 Pontedera (Pisa), Italy

[b] Istituto Italiano di Tecnologia, Center for Micro-BioRobotics @SSSA, Viale Rinaldo Piaggio 34, 56025 Pontedera (Pisa), Italy

[c] CNR, Institute of Clinical Physiology, Via Moruzzi 1, 56124 Pisa, Italy

[d] Istituto Italiano di Tecnologia, Center for Nanotechnology Innovation @NEST, Piazza San Silvestro 12, 56127 Pisa, Italy

[e] NEST, Scuola Normale Superiore and Istituto di Nanoscienze-CNR, Piazza San Silvestro 12, 56127 Pisa, Italy

[f] University of Pisa, Dipartimento di Ricerca Traslazionale e delle Nuove Tecnologie in Medicina e Chirurgia, Via S. Zeno 31, 56126 Pisa, Italy

[g] National Institute for Materials Science (NIMS), International Center for Materials Nanoarchitectonics (MANA), Namiki 1-1, 305-0044 Tsukuba (Ibaraki), Japan

[h] Politecnico di Torino, Department of Mechanical and Aerospace Engineering, Corso Duca degli Abruzzi 24, 10129 Torino, Italy

E-mail: antonella.rocca@sssup.it.it; gianni.ciofani@polito.it

Abstract

Background. Boron nitride nanotubes (BNNTs) represent a new opportunity for drug delivery and clinical therapy. The present work has the objective to investigate pectin-coated BNNTs (P-BNNTs) for their biocompatibility on macrophage cultures, since these cells are among the first components of the immune system to interact with administered nanoparticles.

Methods. As first step, the potential toxicity of P-BNNTs is verified in terms of proliferation, oxidative stress induction and apoptosis/necrosis phenomena. Thereafter, the modulation of immune cell response following P-BNNT exposure is evaluated at gene and protein level, in particular focusing on cytokine release. Finally, P-BNNT internalization is assessed through transmission electron microscopy and confocal microscopy.

Results. The results proved that P-BNNTs are not toxic for macrophages up to 50 µg/ml after 24 h of incubation. The cytokine expression is not affected by P-BNNT administration both at gene and protein level. Moreover, P-BNNTs are internalized by macrophages without impairments of the cell structures.

Conclusions. Collected data suggest that P-BNNTs cause neither adverse effects nor inflammation processes in macrophages.

General significance. These findings represent the first and fundamental step in immune compatibility evaluation of BNNTs, mandatory before any further pre-clinical testing.

Keywords: Boron nitride nanotubes; macrophages; immune system; cytocompatibility

1. Introduction

Boron nitride nanotubes (BNNTs) have intensively been explored over the last 20 years due to their extraordinary properties, that include oxidation and heat resistance, notable hydrophobicity, good electrical insulation in combination with high thermal conductivity, and piezoelectricity [1]. These features make BNNTs suitable for many applications ranging from the automotive and aerospace sectors to the biomedical field. Furthermore, the combination of these nanotubes with engineered materials and systems improves the efficiency of new products [2, 3].

Biomedical field takes advantage of BNNTs for many applications, including pH sensing [4], fabrication of advanced implants [5], bioimaging [6], and electrical stimulation [7]. Moreover, BNNTs have been also proposed as nanocarriers for biomolecules as DNA [8] and for anticancer-drugs [9]. Toxicological investigations demonstrated that BNNTs exhibit optimal biocompatibility with several cell lines such as myoblasts, human neuroblastoma cells, pheochromocytoma cells [7] and endothelial cells [10]. According to Li *e al.*, not only BNNTs are safe in mesenchymal stem cells, but indeed they are able to improve their commitment towards osteoblasts [11]. Chen *et al.* compared the cytocompatibility of carbon nanotubes (CNTs) and BNNTs on human embryonic kidney 293 cells, confirming that CNTs cause apoptosis and prevent proliferation, while BNNTs do not induce any toxic effects [8]. Very recently, Emanet *et al*. extensively investigated carbohydrate-modified BNNTs, highlighting different up-take and toxicity profiles in cancer cells with respect to normal cell lines, further corroborating the potentiality of BNNTs in cancer therapy [12].

In vivo biocompatibility evaluations are still relatively rare. One of the first animal studies reported on the biodistribution of BNNTs functionalized with glycol chitosan and radiolabeled with ^{99m}Tc [13]. This study confirmed the non-toxic behavior of BNNTs, which were accumulated in liver, spleen and gut, and were excreted through kidney. Our group

carried out a systematic toxicological analysis of BNNTs in rabbits. The results proved that animals injected with a BNNT dose of 10 mg/kg until 7 days reveal no harmful effects on liver, kidney, and haematic functionality [14]. More recently, BNNTs were tested on another *in vivo* model, freshwater planarians, in order to assess their effects on *de novo* tissue regeneration [15]. BNNTs, dispersed in gum Arabic solutions, neither caused DNA damage and apoptosis nor interfered with animal regeneration.

Despite several studies demonstrated the biosafety of BNNTs, the examination of the interactions between BNNTs and immune system is still missing, and their immune toxicity investigation is absolutely compulsory before any progress into pre-clinical studies. Macrophages, the phagocytic cells of the immune system, frequently first internalize nanoparticles which could produce undesirable effects on immune system [16]. Many nanoparticles, even though biocompatible, can activate an inflammatory response or immunosuppression following interaction with immune cells, thus voiding their *in vivo* testing and further clinical experimentation [17]. Examples of nanoparticles able to induce immune stimulation include titanium dioxide nanoparticles [18], zinc oxide nanoparticles [19], silica nanoparticles [20], and silver nanoparticles [21]. CNTs, moreover, have been proven to induce inflammation and granulomas into the abdominal cavity of mice [22].

All these data suggest the necessity of a great care introducing innovative nanoparticles in clinical trials, with particular attention to be given to their immune compatibility. The present work represents the first investigation on immunomodulation mediated by BNNTs, a necessary requirement to further exploit BNNTs as therapeutic/diagnosis agent. Pectin-stabilized BNNTs have been tested on RAW 264.7 macrophages and their impact in terms of cytocompatibility and potentially adverse immune reactions has been thoroughly analyzed.

2. Materials and methods

2.1 P-BNNT preparation

High-purity (90%) multi-walled BNNTs were obtained through a carbon-free chemical vapor deposition technique as previously described [23]. 1 mg of BNNTs were dispersed in 1 ml of a solution of apple-derived pectin (Sigma, 1 mg/ml in MilliQ water) and sonicated with an ultrasonic homogenizer (Bandelin) at 8 W for 20 min at 4°C. Thereafter, the dispersion was purified through centrifugation (3 times at 14000 rpm for 5 min) in order to remove excess polymer, and finally the pellet of pectin-wrapped BNNTs (P-BNNTs) was resuspended in MilliQ at a concentration of 1 mg/ml. The characterization of P-BNNTs was carried out using scanning electron microscopy (SEM, Helios NanoLab 600i, FEI) and transmission electron microscopy (TEM, Zeiss Libra 120 Plus). The analysis of particle size distribution and Z-potential was performed by means of a Nano Z-Sizer 90 (Malvern Instrument).

2.2 Cytocompatibility assays

Cytocompatibility of P-BNNTs has been evaluated on mouse macrophages RAW 264.7 (ATCC® TIB71™) at doses in the range 0-50 µg/ml, established basing on previous biological investigations carried out on the same typology of nanotubes [24].

The complete expansion medium of the cells was composed by high-glucose Dulbecco's Modified Eagle's Medium (DMEM), 10% fetal bovine serum, 100 U/ml penicillin, 100 mg/ml streptomycin. The seeding density of cells (at fourth passage) for all the assays was 5000 cells/cm^2. After 24 h from seeding, cells were treated with P-BNNTs in growth medium for 24 h.

WST-1 assay ((2-(4-iodophenyl)-3-(4-nitophenyl)-5-(2,4-disulfophenyl)-2H-tetrazoilium monosodium salt, BioVision) was performed to evaluate cell metabolism. For this test, 10 µl of the WST-1 solution and 100 µl of the fresh medium were incubated with cells seeded in

96-well plates (n = 6) for 90 min and then the absorbance of the supernatants was measured at 450 nm with a microplate reader (Victor3, Perkin Elmer).

For the Quant-iT™ PicoGreen® dsDNA assay (Molecular Probes), cell cultures (n = 6) were lysed and incubated with the reagents in dark at room temperature following the manufacturer's instructions. The fluorescence of the solutions was finally measured in 96-well black plates through the microplate reader (excitation 485 nm, emission 535 nm).

Reactive oxygen species (ROS) production was assessed with the 6-carboxy-2',7'-dichlorodihydrofluorescein diacetate bis(acetoxymethyl)-ester (C-DCF-DA; Molecular Probes), which is converted in its fluorescent form by ROS. Cells, seeded in 12-well plates (n = 6), were washed with Hanks'-buffered saline and incubated for 30 min with C-DCF-DA (25 μM) at 37°C in Hank's buffer. Thereafter, cells were scraped and resuspended in Hank's buffer and the fluorescence was measured by flow-cytometry (BD Accuri™ C6) at 485 nm excitation and 525 nm emission reading 10000 events for each sample.

Annexin V-FITC Apoptosis Detection kit (Sigma) was used to quantify apoptotic/necrotic cells. Briefly, cells plated in 12-well plates (n = 6) were collected and stained with annexin V-FITC and propidium iodide following the manufacturer's instructions. After 10 min of incubation at room temperature, 10000 events *per* sample were analyzed through flow cytometry.

2.3 Cytokine detection

To estimate the cytokine production following appropriate treatments, RAW 264.7 were seeded in 24-wells plate and after 24 h were incubated with 1 μg/ml of lipopolysaccharides from *Escherichia coli* 055:B5 (LPS, Sigma) as a positive control, or with 5 and 10 μg/ml of BNNTs. Cytokine release was estimated through enzyme-linked immunosorbent assay (ELISA, Millipore), and only for this test the cell seeding density was 100000 cells/cm^2. Cell

culture supernatants were harvested after the treatment in order to detect interleukin 6 (IL-6), interleukin 10 (IL-10) and tumor necrosis factor α (TNF-α) according to the manufacturer's protocol. Moreover, cells were collected and processed through Pierce™ BCA Protein Assay Kit (Fisher Scientific) to determine the total cellular protein content, which was used to normalize the concentration of cytokines of each sample (n = 6).

Quantitative real time RT-PCR (qPCR) was performed for gene transcription analysis. At the end of the treatment, the cells, seeded in 24-wells plates (n = 6), were lysed to extract the RNA with the RNeasy® Plus Mini kit (QIAGEN) using the automated robotic workstation QIAcube (QIAGEN). Following the assessment of RNA purity and concentration with a Nanodrop spectrophotometer (Thermo Scientific), RNA (500 ng) was reverse-transcribed by using the iScriptTM Reverse Transcription Supermix (Bio-Rad). The obtained cDNA was amplified through the Cytokines & Chemokines RT^2 Profiler PCR Array (Qiagen, PAMM-150Z). The program temperature performed on the thermocycler CFX Connect™ Real-Time PCR Detection System (Bio-Rad) was the following: one cycle at 95°C for 10 min, 40 cycles at 95°C for 15 s and 60°C for 1 min, and finally a temperature ramp from 65°C to 95°C, with 0.5°C/s increments. The $\Delta\Delta Ct$ method was used for the relative quantification of the target genes. The gene list of the 84 target genes and 5 reference genes analyzed is reported in Table S1 of Supplementary Material.

2.4 P-BNNT / RAW 264.7 interaction assessment

SEM observations were performed to qualitatively analyze the cell shape and surface following P-BNNT treatments. After a 24 h incubation with 10 µg/ml of P-BNNTs, cultures were fixed with 4% paraformaldehyde in PBS for 30 min at 4°C and then with 2.5% glutaraldehyde in de-ionized water for 2 h at 4°C. After dehydration in a series of increasing ethanol concentrations and air-drying, the samples were sputter-coated with a thin gold layer and observed using SEM.

TEM was performed on a Zeiss Libra 120 Plus instrument operating at 120 kV and equipped with an in-column omega filter. Control and treated (10 µg/ml P-BNNTs for 24 h) macrophage cultures were fixed as monolayers with a solution of 1.5% glutaraldehyde in cacodylate buffer. Thereafter, cells were scraped, centrifuged, and treated as pellets with a standard embedding protocol. Briefly, samples were post-fixed in 2% osmium tetroxide in cacodylate buffer, rinsed and stained *en bloc* with 3% uranyl acetate solution in 20% ethanol. Finally, samples were dehydrated and embedded in epoxy resin (Epon 812, Electron Microscopy Science), that was baked for 48 h at 60°C. Thin sections of 90 nm thickness were cut with a UC7 Leica ultramicrotome and collected on 300 meshes copper grids.

To verify the P-BNNT uptake by macrophages, laser scanning confocal microscopy was carried out. Cells, plated on Ibidi 60 µ-Dish (35 mm), were treated with 10 µg/ml of P-BNNTs and fixed after 24 h with 4% paraformaldehyde in PBS for 30 min at 4°C. Standard staining of f-actin and cell nucleus was performed with Oregon Green® 448 phalloidin (5 µl each 200 µl of medium) and Hoechst 33342 (1 µl each 1 ml of medium), respectively. Cultures were finally observed under confocal microscope (C2s, Nikon). P-BNNT observation was possible by exciting sample at 642 nm and collecting emitted fluorescence between 670 nm and 750 nm.

Co-localization of P-BNNTs with lysosomes was evaluated through the LysoTracker® staining (Molecular Probes). Cells, at the end of the P-BNNT treatment (10 µg/ml for 24 h), were incubated with 100 nM of the lysosome probe and with Hoechst 33342 for 1 h, and then observed under confocal microscope.

Stiffness of cell membrane was evaluated through SICM as described by Marino *et al.* [25]. Briefly, 200 nm borosilicate glass pipettes were mounted on a piezo-translator stage (Nanocube P-611 3S with a driver E-664, Physik Instrumente). A pressure (ΔP) was applied by a syringe controlled by a micrometric screw. When the pipette approached a sample along

the *Z* axis, a current decrease occurred because of a smaller conducting space. The pipette was stopped when the ion current (*I*) has been reduced to a preset percentage of its maximum value (I_0, measured far enough from the sample). Local elastic modulus was deduced by recording the ion current as a function of the vertical pipette position (*I/Z* curve). Signals were filtered thanks to a low-pass filter (400 Hz). The LabVIEW 8.2.1 software was used for both the scan control and the data analysis. Eight cells *per* experimental condition were analyzed, and Young's modulus was measured in 4 different points of each cell, in the perinuclear zone, by applying a stress ΔP = 3000 Pa.

2.5 Statistical analysis

Statistical analysis was performed through KaleidaGraph (Sinergy Software) using one-way ANOVA followed by Bonferroni's *post-hoc* test, while qPCR results were analyzed with Bio-Rad CFX Manager software. Data distributions from SICM were tested with the Shapiro normality test, and subsequently with Wilcoxon signed-rank test. All data were considered statistically significant at *p*-values < 0.05.

3. Results

3.1 Pectin-coated BNNTs

P-BNNTs are well dispersed in aqueous solutions, as demonstrated by SEM images at low (Figure 1a) and high (Figure 1b) magnification. TEM imaging highlighted the typical shape of multi-walled BNNTs (Figure 1c) and electron diffraction pattern showed the hexagonal structure of layers comprising them (Figure 1d).

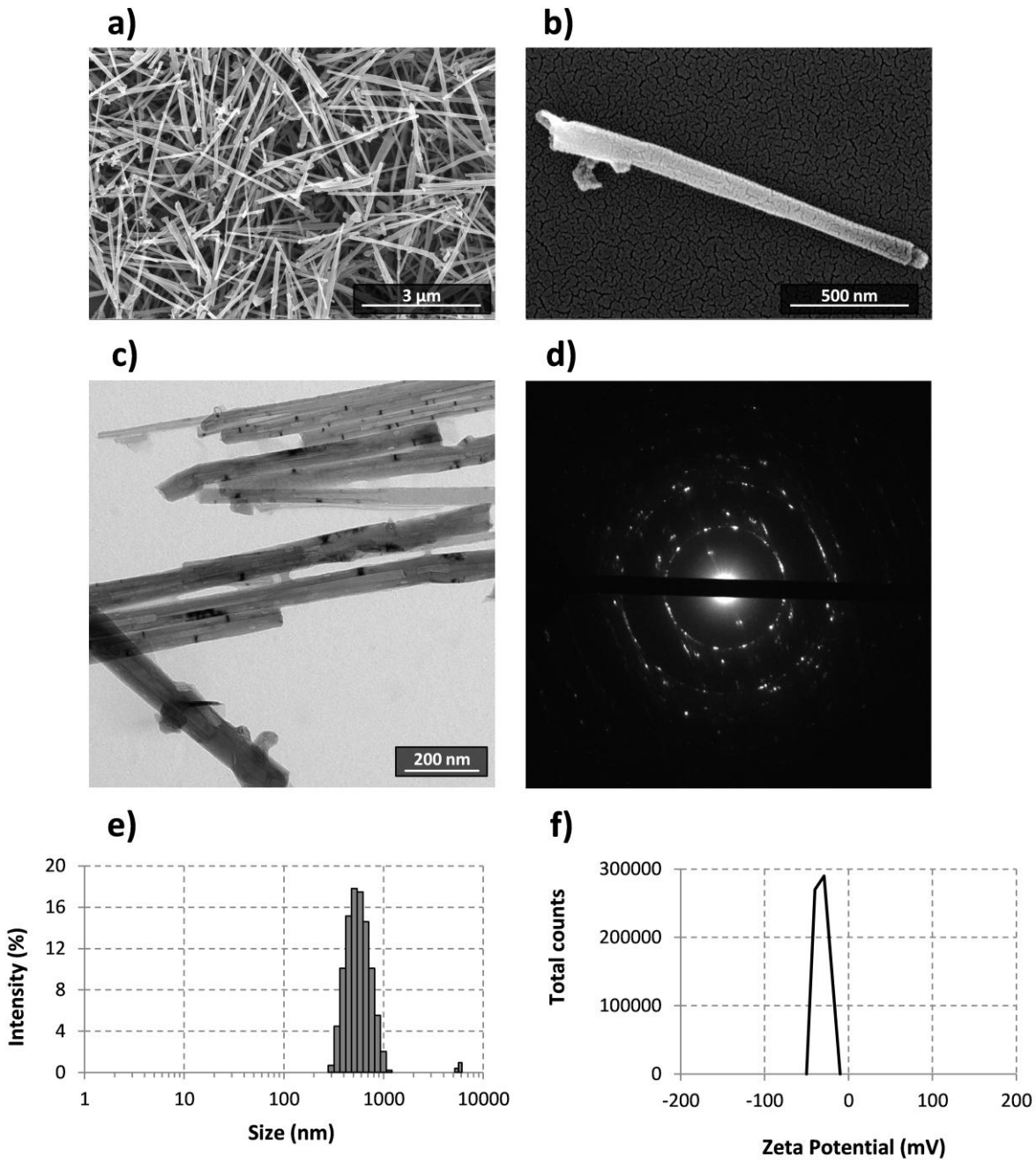

Figure 1. SEM imaging of P-BNNTs at low (a) and high (b) magnification. Morphology and structure of P-BNNTs are confirmed by TEM bright field image (c) and electron diffraction pattern (d). Dynamic light scattering (e) and Z-potential (f) analysis of P-BNNT dispersions.

The hydrodynamic diameter (D_H) distribution obtained by dynamic light scattering is reported in Figure 1e, and presents an average value of about 500 nm. The model described by Nair *et al.* [26] has been used for the estimation of the average nanotube length L corresponding to the experimental D_H, by exploiting the following equation:

$$D_H = \frac{L}{\ln(\frac{L}{d}) + 0.32} \quad (1)$$

where d is the diameter of the nanotube (d = 50 nm). By using this equation we obtained an average P-BNNT length of 2.0 µm (with a range of 1.0 - 4.0 µm), confirming qualitative evidences provided by the SEM and TEM observations.

The Z-potential resulted -33.3±6.0 mV (Figure 1f), highlighting an excellent stability of the dispersion even after several months since the preparation. Energy-filtered transmission electron microscopy (EFTEM), provided in Supplementary Material, confirmed the presence of a pectin layer wrapping the BNNTs, suggested by the presence of carbon surrounding the P-BNNTs that stabilizes the nanotubes in aqueous solution (Figure S1).

3.2 Pectin-coated BNNT cytocompatibility

Cytocompatibility tests were performed to evaluate P-BNNT effects on proliferation and viability of macrophages after an acute 24 h treatment with increasing concentrations of nanotubes (0, 5, 10, 20 and 50 µg/ml).

WST-1 results demonstrated that cell metabolism is not altered by P-BNNT treatment at all the considered concentrations ($p > 0.05$) with respect to the control cultures (Figure 2). Proliferation rate was assessed using Quant-iT™ PicoGreen® dsDNA assay, enabling the quantification of the total dsDNA in the cultures. Once again, obtained data indicate no differences in terms of DNA concentration (and, therefore, of cell number) in the treated samples ($p > 0.05$ in all the cases, Figure 2).

Flow-cytometry assessment of ROS production following P-BNNT administration further corroborated the hypothesis of absence of negative effects: after a 24 h exposure, ROS levels in all the treatments were statistically non-different from the control cultures ($p > 0.05$ in all the cases, Figure 2).

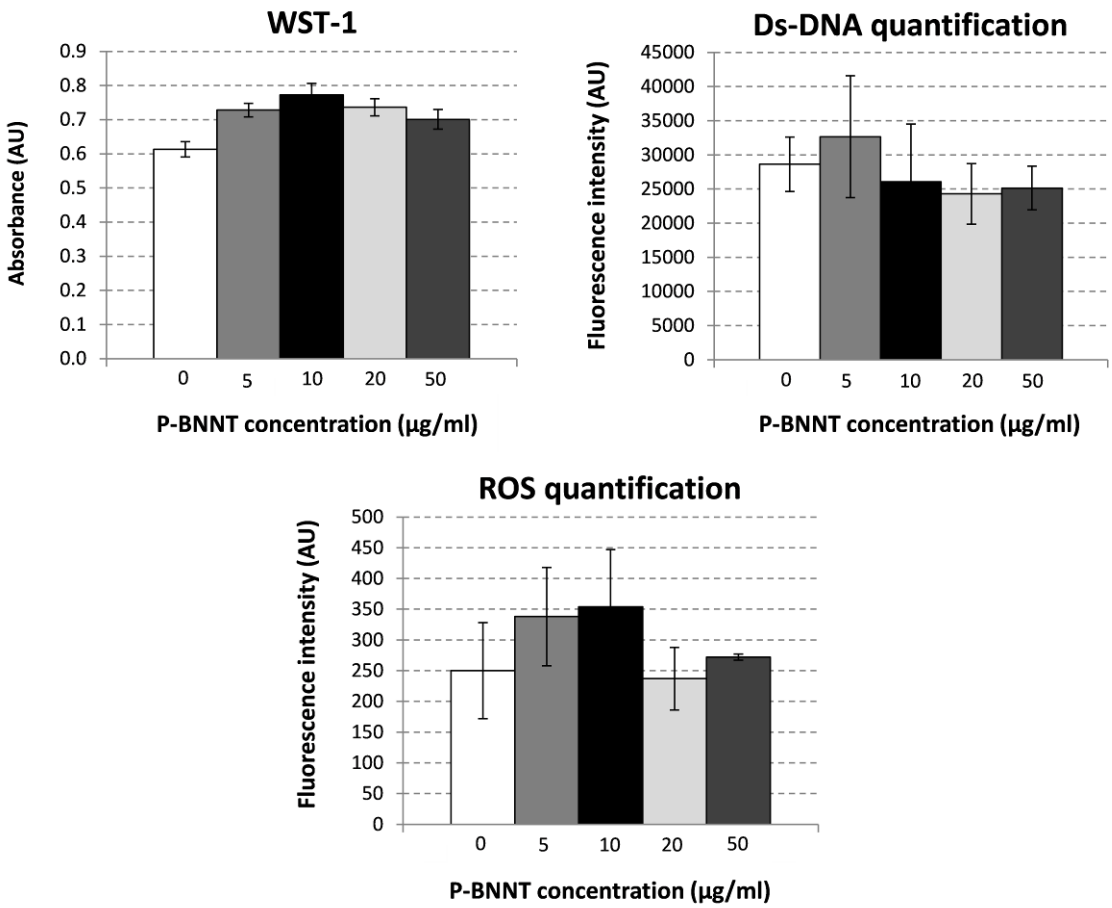

Figure 2. Cytocompatibility evaluation on RAW 264.7 macrophages following incubation with 0-50 µg/ml of P-BNNTs for 24 h: metabolic activity, ds-DNA content in cultures, ROS production.

Flow-cytometry quantification of necrotic/apoptotic phenomena finally demonstrated that an acute treatment with P-BNNTs, up to 50 µg/ml, do not cause a statistically significant increase of necrotic, early apoptotic and late apoptotic cells in comparison to control culture ($p > 0.05$). Scatter plots of a representative experiment are depicted in Figure 3, while detailed quantifications are reported in Table 1.

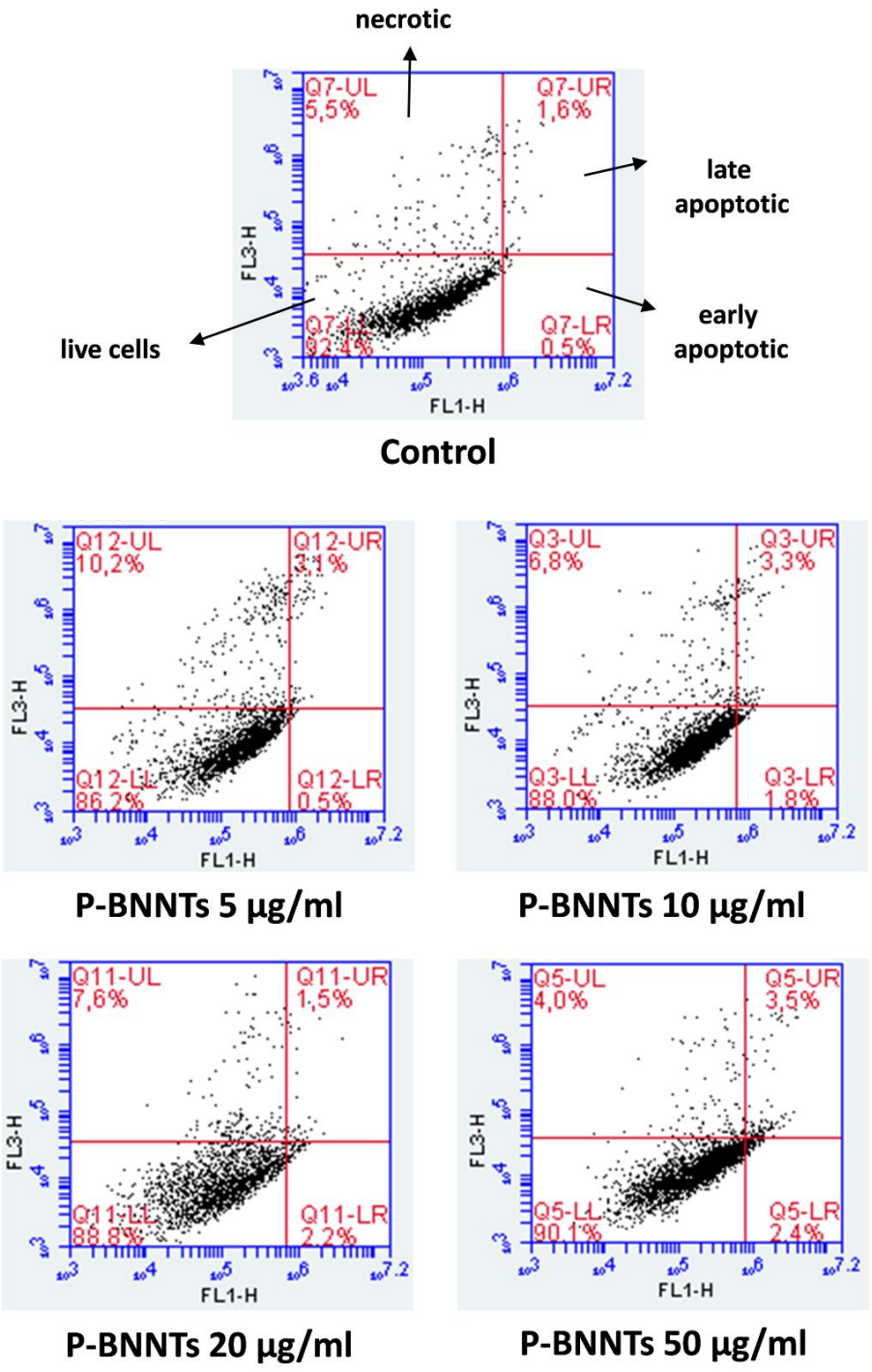

Figure 3. Flow-cytometry evaluation of apoptosis in RAW 264.7 macrophages treated for 24 h with 0-50 µg/ml of P-BNNTs.

P-BNNT concentration (µg/ml)	Viable cells (%)	Necrotic cells (%)	Early apoptotic cells (%)	Late apoptotic cells (%)
0	92.1±0.1	5.8±0.6	0.3±0.2	1.8±0.3
5	85.3±3.2	11.5±2.0	0.7±0.1	2.5±0.3
10	88.8±0.7	7.8±1.3	1.0±1.0	2.2±1.5
20	89.0±0.1	7.4±0.1	2.2 ±0.1	1.5±0.1
50	92.0±2.4	4.4±0.6	1.5 ±1.2	2.1±1.7

Table 1. Quantification of viable, necrotic, early apoptotic, and late apoptotic cells after 24 h of incubation with increasing concentrations of P-BNNTs.

3.3 Effects of P-BNNTs on immune response

The potential immunomodulation effects of P-BNNTs on macrophages have been investigated through ELISA to assess the cytokine release, and through qPCR for the analysis of transcription of cytokine and chemokine genes. We decided to evaluate 5 and 10 µg/ml of BNNTs for all the subsequent experiments, *i.e.*, safe concentrations which are one order of magnitude lower with respect to the maximum concentration tested in the cytocompatibility assays. Macrophages have been thus treated for 24 h with P-BNNTs or stimulated with lipopolysaccharides (LPS, 1 µg/ml) as positive control, and the effects were compared to the behavior of non-treated control cultures. The results obtained from ELISA (Figure 4a) revealed that IL-6 secretion normalized to the total protein content was not significantly affected by both concentrations of P-BNNTs with respect to the control (88±35 pg/µg for P-BNNTs 5 µg/ml, 69±16 pg/µg for P-BNNTs 10 µg/ml, 67±47 pg/µg for the control), while significant release occurred in the LPS-treated culture (5.965±0.746 ng/µg, $p < 0.05$). Also in the case of IL-10 release, P-BNNTs did not cause statistically significant alterations in comparison with untreated cultures (0.729±0.311 ng/µg for P-BNNTs 5 µg/ml, 1.270±0.829 ng/µg for P-BNNTs 10 µg/ml, 0.682±0.073 ng/µg for the control; on the contrary

28.679±2.544 ng/µg for LPS treatment, $p < 0.05$). Finally, P-BNNT treatment did not significantly alter even the release of TNF-α in macrophages treated with both 5 µg/ml (6.929±0.069 ng/µg) and 10 µg/ml (7.398±0.169 ng/µg) of P-BNNTs with respect to the control (5.749±0.086 ng/µg). Also in this case, LPS caused instead a significant release of TNF-α (21.118±5.091 ng/µg, $p < 0.05$).

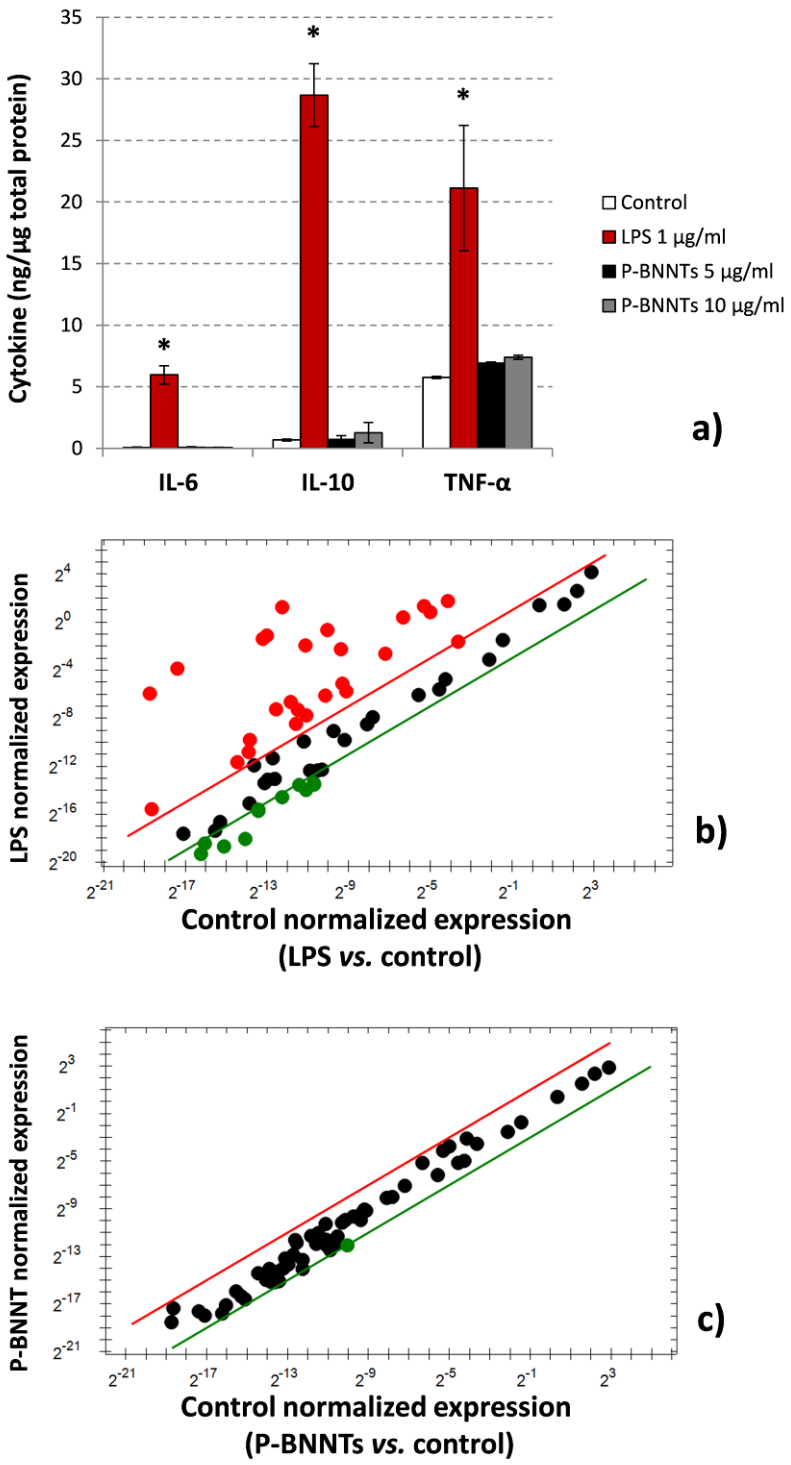

Figure 4. Cytokine release from macrophages incubated for 24 h with 5 and 10 μg/ml of P-BNNTs or with 1 μg/ml of LPS and compared to control cultures (* $p < 0.05$) (a). Scatter plots of up- (in red) and down- (in green) regulated genes in RAW 264.7 stimulated with 1 μg/ml of LPS (b) or with 10 μg/ml of P-BNNTs (c) with respect to control cultures (regulation threshold 4.0).

Figure 4b-c shows the results of the transcription profile of the main cytokine and chemokine genes involved in an immune reaction. Gene transcription levels are reported as scatter data depicted in red for up-regulated genes, in green for down-regulated genes, and in black for no significant change in transcription level. Lines show the 4-fold up- (red) and down- (green) regulation threshold. The comparison control *vs.* P-BNNT treatment (Figure 4b) at the highest concentration (10 μg/ml) demonstrated that P-BNNTs did not induce statistically significant changes in the transcription level of the 84 analyzed genes, except for interleukin 1β (*Il1b*) which was significantly down-regulated (4.1 folds, $p < 0.05$). Conversely, the LPS treatment caused statistically significant up-regulation of 26 genes and down-regulation of 11 genes related to the immune response with respect to the non-treated cultures (Figure 4c, $p < 0.05$). Table 2 shows the list of the investigated genes along with the up- or down-regulation fold.

Target	**Fold difference with respect to the control**	
	LPS (1 μg/ml)	**P-BNNTs (10 μg/ml)**
Adipoq	-5.2*	-2.0
Bmp6	-1.1	-1.6
Bmp7	-2.54	-2.1
Cd1	-15.9*	-1.9
Cd11	-1.3	1.9
Cd12	39.3*	1.6

Cd17	-1.2	-1.1
Cd2	100.0*	2.2
Cd22	8.6*	-1.3
Cd24	-6.5*	-1.9
Cd3	59.6*	2.1
Cd4	105.6*	2.3
Cd5	139.5*	-1.5
Cd7	579.2*	1.8
Cntf	-3.9	1.1
Csf1	8.5*	-1.1
Csf2	9.9*	-1.9
Csf3	3800.9*	-1.6
Ctf1	8.6*	2.4
Cx3cl1	-2.8	-2.9
Cxcl1	6.9*	1.1
Cxcl10	-2.1	-1.5
Cxcl13	-4.5*	-1.8
Cxcl16	-2.0	-1.3
Cxcl3	11596.1*	-3.5
Gpi1	-1.1	-1.2
Ifna2	-4.4*	-1.1
Il10	18.2*	-1.1
Il11	16.4*	-2.4
Il15	1.6	1.1
Il16	-1.3	1.1
Il17f	-1.4	-1.6
Il18	-1.4	-1.5

Il1a	3609.1*	-1.7
Il1b	670.2*	-4.1*
Il1rn	57.1*	2.4
Il2	-3.6	-1.3
Il23a	3.3	-2.9
Il27	18.4*	1.4
Il4	-7.1*	-2.5
Il5	-4.9*	-3.3
Il6	11760.3*	-1.2
Il7	2.6	-1.1
Il9	-3.5	-1.7
Lif	36.5*	1.5
Lta	2.4	-1.5
Ltb	-1.1	-1.1
Mif	-1.1	-1.1
MStn	-8.3*	-2.9
Nodal	-1.4	-1.8
Osm	16.3*	1.1
Pf4	23.8*	1.1
PPbp	7090.9*	1.2
Spp1	2.4	-1.1
Thpo	-4.9*	-2.1
Tnf	4.0*	1.1
Tnfrsf11b	-11.9*	-2.8
Tnfsf10	-7.4*	-1.4
Tnfsf11	-2.3	-1.8
Tnfsf13b	-1.5	1.1

Vegfa	10.3*	-1.1

Table 2. List of up- or down-regulated genes following treatment with LPS or P-BNNTs with respect to the control. (* $p < 0.05$).

3.4 P-BNNTs / macrophages interaction

Nanotubes/macrophages interactions have been investigated through SEM, TEM and confocal microscopy after a 24 h treatment with 10 µg/ml of P-BNNTs. Mechanical properties of the cells following P-BNNT uptake have been evaluated with scanning ion conductance microscopy (SICM).

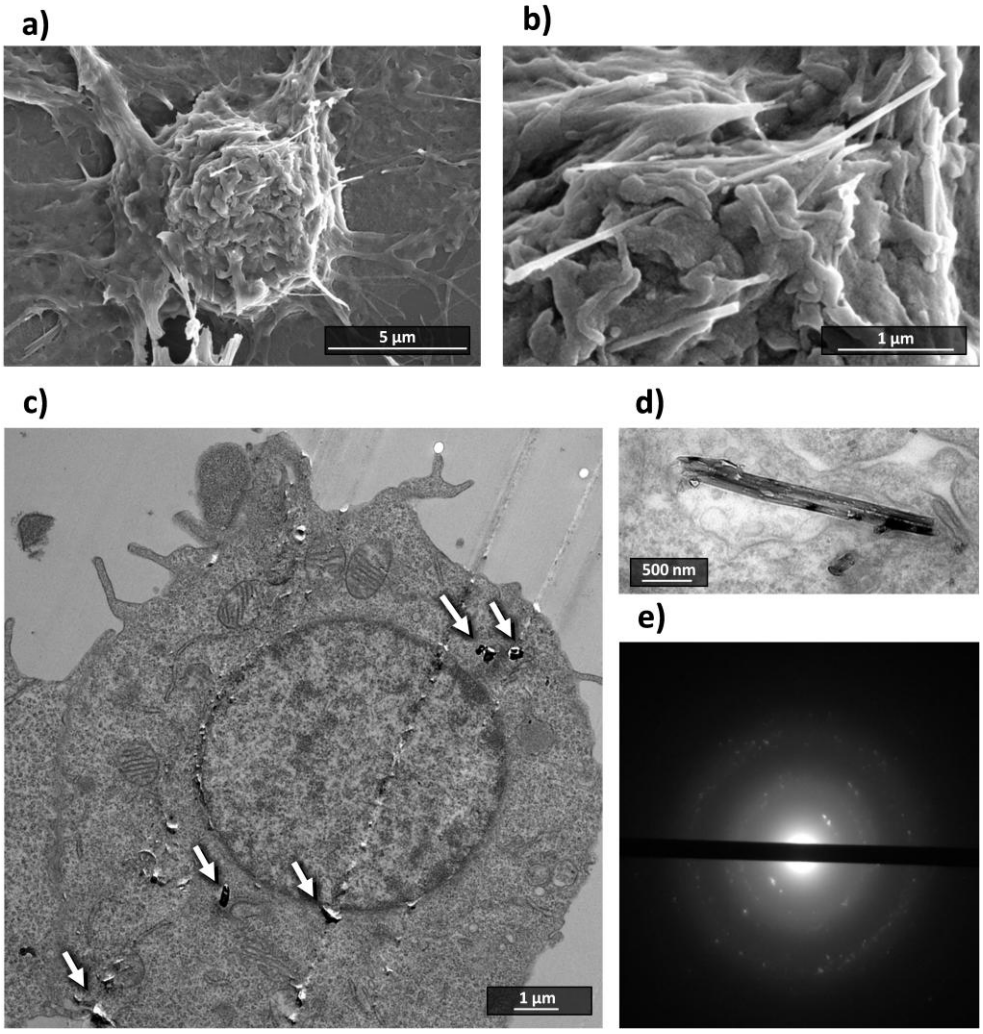

Figure 5. SEM images of macrophages incubated with 10 µg/ml of P-BNNTs for 24 h at low (a) and high (b) magnification. TEM image of the same culture showing P-BNNT internalization (white

arrows indicate single and aggregated P-BNNTs) at low (c) and high (d) magnification; electron diffraction pattern of P-BNNTs inside the cells (e).

SEM images showed that P-BNNTs do not qualitatively affect the morphology of macrophages with respect to control cultures (Figure 5a, control not shown). Moreover, the images at higher magnification (Figure 5b) demonstrated the presence of nanotubes strictly entrapped in membrane protrusions.

TEM analysis revealed that about 65% of treated cells appear positive for the internalization of P-BNNTs, that formed small aggregates (from one to three nanotubes) in the perinuclear regions of the cytoplasm (Figure 5c). Figure 5d shows P-BNNTs inside the cell at higher magnification, while in Figure 5e the correspondent electron diffraction pattern confirms the structure of internalized P-BNNTs.

Laser scanning confocal microscopy further confirmed the P-BNNT internalization by macrophages. Figure 6a reveals single channel and merged image of a single confocal acquisition and side projections of a confocal Z-stack, demonstrating P-BNNT internalization in the cell cytoplasm (actin in green, P-BNNTs in red, nuclei in blue). Finally, LysoTracker® staining highlighted that P-BNNTs do not co-localize with lysosomes (quantitative evaluation showed a Pearson's coefficient R = 0.14), as suggested by Figure 6b, showing 3D rendering of acquisitions of lysosomes (in green), P-BNNTs (in red) and nuclei (in blue).

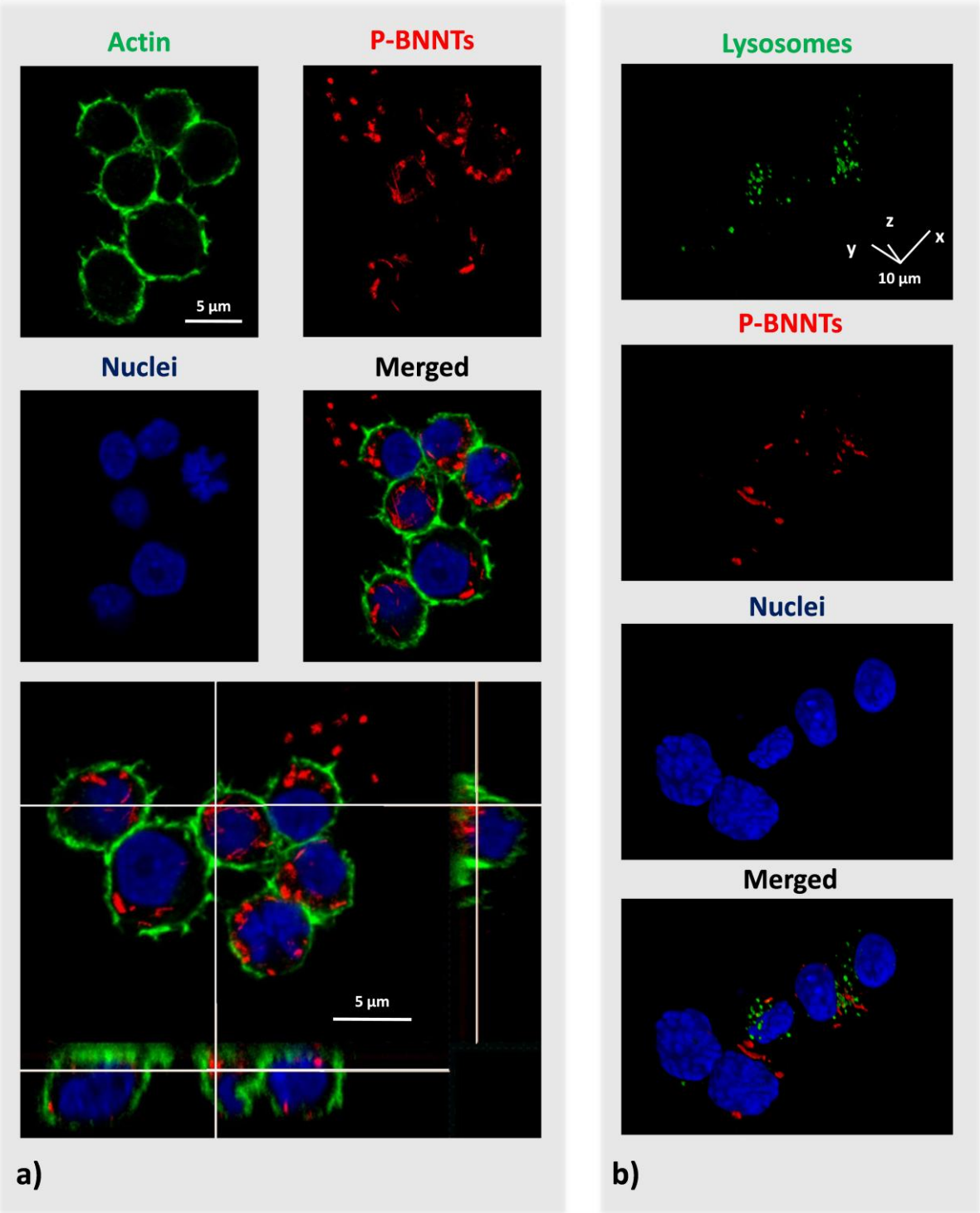

Figure 6. Laser confocal analysis of P-BNNT uptake: f-actin in green, P-BNNTs in red, nuclei in blue (a); 3D rendering of lysosomes / P-BNNTs co-localization investigation: lysosomes are shown in green, P-BNNTs in red, nuclei in blue (b).

SICM analysis eventually highlighted a change in cell membrane mechanical properties upon P-BNNT internalization. Macrophages undergone a 24 h treatment with 10 µg/ml of P-

BNNTs (and thus extensively internalizing them) presented a membrane Young's modulus E = 2375±680 kPa, significantly increased if compared to that one of the control cells (840±335 kPa).

4. Discussion

The aim of this work is to provide preliminary data about BNNT immune compatibility, thus our investigation has been focused on the assessment of the effects of BNNTs on RAW 264.7 macrophages.

In order to improve water-stabilization of highly hydrophobic BNNTs, we successfully exploited pectin as a wrapping polymer. Pectin is a natural polysaccharide of vegetable origin composed by D-galacturonic acid units [27], widely exploited for the stabilization of different kinds of nanomaterials in aqueous environments, including silver nanoparticles [28] and silica-coated magnetic nanoparticles [29], and as bulk material for the preparation of nanocarriers for drug delivery [30]. The issue of low water dispersibility of BNNTs is object of intensive research, that led to the exploitation of several approaches including PEGylated phospholipids, glycol chitosan, flavin mononucleotides, *etc.* [7]. Here, the use of pectin as a surfactant was found to considerably improve the water dispersion and stability of BNNTs, which were stable for several months since the preparation (no variation in terms of hydrodynamic size distribution and *Z*-potential).

Once the stability of P-BNNTs has been confirmed, experiments were directed to the cytocompatibility examination of P-BNNTs on mouse macrophages RAW 264.7. Macrophages have been selected for this study as they are the first cells of the immune system encountered by nanoparticles in mammals [16]. The cell viability assessment demonstrated that P-BNNTs do not cause adverse effects on macrophage culture after 24 h of treatment up

to 50 μg/ml. Moreover, necrotic/apoptotic phenomena and oxidative stress production were excluded as well. These data are in contrast with the results of Horvàth *et al.*, which showed BNNT cytotoxicity in several cell lines, including macrophages, already at low concentrations (2 μg/ml). However, this cell impairment was probably due to the use of long nanotubes (10 μm), known to elicit strong toxic reactions during the cellular internalization process [31].

For the first time, we approached immune compatibility of BNNTs. The immune system protects the organism in first instance owing to phagocytic cells (among which macrophages), that take up harmful agents and release cytokines to preserve body homeostasis [32]. Nanoparticles, once internalized by immune cells, are rapidly excreted from the systemic circulation, that decreases their availability at the target site [33]. Moreover, cytokine secreted by immune cells as a consequence of a foreign body reaction could start a harmful inflammation process for the organism [34]. Several kinds of nanoparticles that induce adverse immune reactions were reported in the literature. As an example, titanium dioxide nanoparticles (up to 10 mg/kg) which were daily injected in mice for 90 days caused inflammation of kidneys, as demonstrated by the increment of inflammatory cytokines, such as TNF-α, MIF, IL-2, IL-4, IL-6, IL-8, IL-10, IL-18, IL-1β, TGF-β, INF-γ, both at gene and protein level [35]. Aluminum oxide nanoparticles, after 24 h since a single administration (10 mg/kg) in mice, were proven to increase the blood level of IL-8 in comparison to the control animals [36]. It is therefore clear that a lack of undesirable inflammatory response is a priority for the application of nanoparticles in clinical treatments.

In our study the analysis of the typical cytokines involved in the immune response was performed through ELISA and qPCR. The exposure to P-BNNTs for 24 h does not affect cytokine (IL-6, IL-10, TNF-α) release by macrophages. IL-6 is produced by macrophages in response to pathogens [37], activating a pro-inflammation cascade signaling together with TNF-α, which is the master regulator of pro-inflammatory cytokines production [38]. IL-10 is

an anti-inflammatory cytokine which restricts the immune response to danger agents in order to avoid damage to the organism [39].

Similarly to the ELISA results, the gene panel analysis revealed a marked difference among control and LPS-treated cultures. In particular, as expected, the LPS stimulation activates a molecular signaling typical of an inflammatory state [39-41]. The up-regulated genes comprise pro-inflammatoty cytokines (*Tnfa, Il1a, Il1b, Il1rn, Il6, Il27*), anti-inflammatory cytokines (*Il10, Il11*), chemokines (*Ccl2, Ccl2, Ccl22, Ccl3, Ccl4, Ccl5, Ccl7, Cxcl1, Cxcl3, Pf4, Ppbp*), and growth factors (*Csf1, Csf2, Csf3, Lif, Osm, Vegfa*). Among the down-regulated genes we find chemokines (*Ccl1, Ccl24, Cxcl1*), interferon (*Ifna2*), interleukins (*Il4, Il5*), TNF receptors (*Tnfrsf11b, Tnfsf10*), and growth factors (*Adipoq, MStn, Thpo*). Conversely, no significant variations in gene transcription were observed following the P-BNNT treatment, except for the down-regulation of the pro-inflammatoty cytokine *Il1b*. *Il1b* is secreted by activated macrophages and plays a key role in supporting phagocytosis of foreign bodies [42]. In a similar case, citrate-stabilized gold nanoparticles were found to inhibit *Il1b* and its down-stream responses both *in vitro* and *in vivo* [43]. Even though we are far to make any hypothesis about anti-inflammatory response following the administration of P-BNNTs (as we do not have significant reduction of any other inflammation marker), the decreasing expression of *Il1b* is interesting and worth of further investigations.

Concerning P-BNNT/cell interaction, SEM observation demonstrated that P-BNNTs are strongly interacting with the cell membrane, resulting the nanoparticles extensively entrapped by microvilli. Upon internalization, nanotubes are confined within the endoplasmic compartment, without affecting the cell ultrastructure as confirmed by both TEM and confocal microscopy. BNNT internalization was well documented in many different kinds of cells [7], and in the case of RAW 264.7 we also confirmed an extensive nanoparticle uptake.

The lack of co-localization with lysosomes, however, suggests an early stage of the internalization process.

Finally, we assessed mechanical properties of the cells following P-BNNT treatment, and SICM measurements revealed a considerably stiffer membrane in treated cells with respect to the controls. Conversely, in the literature it has been reported that nanoparticles can induce a reduction of membrane stiffness, as highlighted for manganese ferrite nanoparticles tested on RAW 264.7 [44]. In this study Roduit *et al.* performed AFM analysis on macrophages, suggesting that the membrane stiffness is reduced following a depolymerization of the cytoskeletal actin, necessary to increase the motility of the cells during the phagocytosis process. Our results are instead in line with the data previously obtained on stem cells treated with barium titanate nanoparticles [45], suggesting that a remodeling of the cytoskeleton following nanoparticle internalization leads to an increased membrane stiffness because of an increment of actin filaments surrounding the nanoparticles being internalized.

5. Conclusion

Potential immune response caused by nanoparticles should be carefully considered before any further exploitation in nanomedicine. This study preliminarily assessed immune compatibility of boron nitride nanotubes toward macrophage cultures. Overall, our data indicate that P-BNNTs neither alter the macrophage growth no cause apoptosis and oxidative stress. Moreover, P-BNNTs, once internalized by cells, do not stimulate inflammation response both at protein and gene levels. In our opinion these results are extremely important, since they represent an encouraging fundamental step toward further preclinical testing of BNNTs.

References

[1] S. Kalay, Z. Yilmaz, O. Sen, M. Emanet, E. Kazanc, M. Culha, Synthesis of boron nitride nanotubes and their applications, Beilstein J Nanotechnol 6 (2015) 84-102.
[2] N.G. Chopra, R.J. Luyken, K. Cherrey, V.H. Crespi, M.L. Cohen, S.G. Louie, A. Zettl, Boron nitride nanotubes, Science 269 (1995) 966-967.
[3] D. Golberg, Y. Bando, C.C. Tang, C.Y. Zhi, Boron Nitride Nanotubes, Advanced Materials 19 (2007) 2413-2432.
[4] Q. Huang, Y. Bando, L. Zhao, C.Y. Zhi, D. Golberg, pH sensor based on boron nitride nanotubes, Nanotechnology 20 (2009) 0957-4484.
[5] D. Lahiri, V. Singh, A.P. Benaduce, S. Seal, L. Kos, A. Agarwal, Boron nitride nanotube reinforced hydroxyapatite composite: mechanical and tribological performance and in-vitro biocompatibility to osteoblasts, J Mech Behav Biomed Mater 4 (2011) 44-56.
[6] Z. Gao, C. Zhi, Y. Bando, D. Golberg, T. Serizawa, Noncovalent functionalization of disentangled boron nitride nanotubes with flavin mononucleotides for strong and stable visible-light emission in aqueous solution, ACS Appl Mater Interfaces 3 (2011) 627-632.
[7] G. Ciofani, S. Danti, G.G. Genchi, B. Mazzolai, V. Mattoli, Boron nitride nanotubes: biocompatibility and potential spill-over in nanomedicine, Small 9 (2013) 1672-1685.
[8] X. Chen, P. Wu, M. Rousseas, D. Okawa, Z. Gartner, A. Zettl, C.R. Bertozzi, Boron nitride nanotubes are noncytotoxic and can be functionalized for interaction with proteins and cells, J Am Chem Soc 131 (2009) 890-891.
[9] X. Li, C. Zhi, N. Hanagata, M. Yamaguchi, Y. Bando, D. Golberg, Boron nitride nanotubes functionalized with mesoporous silica for intracellular delivery of chemotherapy drugs, Chem Commun 49 (2013) 7337-7339.
[10] D. Lahiri, F. Rouzaud, T. Richard, A.K. Keshri, S.R. Bakshi, L. Kos, A. Agarwal, Boron nitride nanotube reinforced polylactide-polycaprolactone copolymer composite: mechanical properties and cytocompatibility with osteoblasts and macrophages in vitro, Acta Biomater 6 (2010) 3524-3533.
[11] X. Li, X. Wang, X. Jiang, M. Yamaguchi, A. Ito, Y. Bando, D. Golberg, Boron nitride nanotube-enhanced osteogenic differentiation of mesenchymal stem cells, J Biomed Mater Res B Appl Biomater 12 (2015) 33391.
[12] M. Emanet, O. Sen, Z. Cobandede, M. Culha, Interaction of carbohydrate modified boron nitride nanotubes with living cells, Colloids and surfaces. B, Biointerfaces 134 (2015) 440-446.
[13] D.C. Soares, T.H. Ferreira, A. Ferreira Cde, V.N. Cardoso, E.M. de Sousa, Boron nitride nanotubes radiolabeled with 99mTc: preparation, physicochemical characterization, biodistribution study, and scintigraphic imaging in Swiss mice, Int J Pharm 423 (2012) 489-495.
[14] G. Ciofani, S. Danti, S. Nitti, B. Mazzolai, V. Mattoli, M. Giorgi, Biocompatibility of boron nitride nanotubes: an up-date of in vivo toxicological investigation, Int J Pharm 444 (2013) 85-88.
[15] A. Salvetti, L. Rossi, P. Iacopetti, X. Li, S. Nitti, T. Pellegrino, V. Mattoli, D. Golberg, G. Ciofani, In vivo biocompatibility of boron nitride nanotubes: effects on stem cell biology and tissue regeneration in planarians, Nanomedicine 10 (2015) 1911-1922.
[16] B.S. Zolnik, A. Gonzalez-Fernandez, N. Sadrieh, M.A. Dobrovolskaia, Nanoparticles and the immune system, Endocrinology 151 (2010) 458-465.
[17] B. Fadeel, Clear and present danger? Engineered nanoparticles and the immune system, Swiss Med Wkly 26 (2012) 13609.

[18] A.S. Yazdi, G. Guarda, N. Riteau, S.K. Drexler, A. Tardivel, I. Couillin, J. Tschopp, Nanoparticles activate the NLR pyrin domain containing 3 (Nlrp3) inflammasome and cause pulmonary inflammation through release of IL-1alpha and IL-1beta, Proc Natl Acad Sci U S A 107 (2010) 19449-19454.
[19] V.A. Senapati, A. Kumar, G.S. Gupta, A.K. Pandey, A. Dhawan, ZnO nanoparticles induced inflammatory response and genotoxicity in human blood cells: A mechanistic approach, Food Chem Toxicol 85 (2015) 61-70.
[20] E.J. Park, K. Park, Oxidative stress and pro-inflammatory responses induced by silica nanoparticles in vivo and in vitro, Toxicol Lett 184 (2009) 18-25.
[21] A. Barbasz, M. Ocwieja, J. Barbasz, Cytotoxic Activity of Highly Purified Silver Nanoparticles Sol Against Cells of Human Immune System, Appl Biochem Biotechnol 176 (2015) 817-834.
[22] C.A. Poland, R. Duffin, I. Kinloch, A. Maynard, W.A.H. Wallace, A. Seaton, V. Stone, S. Brown, W. MacNee, K. Donaldson, Carbon nanotubes introduced into the abdominal cavity of mice show asbestos-like pathogenicity in a pilot study, Nat Nano 3 (2008) 423-428.
[23] C. Zhi, Y. Bando, C. Tan, D. Golberg, Effective precursor for high yield synthesis of pure BN nanotubes, Solid State Communications 135 (2005) 67-70.
[24] G. Ciofani, S. Del Turco, A. Rocca, G. de Vito, V. Cappello, M. Yamaguchi, X. Li, B. Mazzolai, G. Basta, M. Gemmi, V. Piazza, D. Golberg, V. Mattoli, Cytocompatibility evaluation of gum Arabic-coated ultra-pure boron nitride nanotubes on human cells, Nanomedicine (London, England) 9 (2014) 773-788.
[25] A. Marino, A. Desii, M. Pellegrino, M. Pellegrini, C. Filippeschi, B. Mazzolai, V. Mattoli, G. Ciofani, Nanostructured Brownian surfaces prepared through two-photon polymerization: investigation of stem cell response, ACS Nano 8 (2014) 11869-11882.
[26] N. Nair, W.J. Kim, R.D. Braatz, M.S. Strano, Dynamics of surfactant-suspended single-walled carbon nanotubes in a centrifugal field, Langmuir 24 (2008) 1790-1795.
[27] B.R. Thakur, R.K. Singh, A.K. Handa, Chemistry and uses of pectin--a review, Crit Rev Food Sci Nutr 37 (1997) 47-73.
[28] Y.L. Balachandran, S. Girija, R. Selvakumar, S. Tongpim, A.C. Gutleb, S. Suriyanarayanan, Differently environment stable bio-silver nanoparticles: study on their optical enhancing and antibacterial properties, PLoS One 8 (2013).
[29] R. Rakhshaee, M. Panahandeh, Stabilization of a magnetic nano-adsorbent by extracted pectin to remove methylene blue from aqueous solution: a comparative studying between two kinds of cross-linked pectin, J Hazard Mater 189 (2011) 158-166.
[30] C.Y. Yu, Y.M. Wang, N.M. Li, G.S. Liu, S. Yang, G.T. Tang, D.X. He, X.W. Tan, H. Wei, In vitro and in vivo evaluation of pectin-based nanoparticles for hepatocellular carcinoma drug chemotherapy, Molecular pharmaceutics 11 (2014) 638-644.
[31] L. Horvath, A. Magrez, D. Golberg, C. Zhi, Y. Bando, R. Smajda, E. Horvath, L. Forro, B. Schwaller, In vitro investigation of the cellular toxicity of boron nitride nanotubes, ACS Nano 5 (2011) 3800-3810.
[32] D.M. Mosser, J.P. Edwards, Exploring the full spectrum of macrophage activation, Nat Rev Immunol 8 (2008) 958-969.
[33] M.A. Dobrovolskaia, P. Aggarwal, J.B. Hall, S.E. McNeil, Preclinical studies to understand nanoparticle interaction with the immune system and its potential effects on nanoparticle biodistribution, Mol Pharm 5 (2008) 487-495.
[34] Q. Jiao, L. Li, Q. Mu, Q. Zhang, Immunomodulation of nanoparticles in nanomedicine applications, Biomed Res Int 426028 (2014) 20.
[35] S. Gui, Z. Zhang, L. Zheng, Y. Cui, X. Liu, N. Li, X. Sang, Q. Sun, G. Gao, Z. Cheng, J. Cheng, L. Wang, M. Tang, F. Hong, Molecular mechanism of kidney injury of mice

caused by exposure to titanium dioxide nanoparticles, J Hazard Mater 195 (2011) 365-370.
[36] E.J. Park, G.H. Lee, C. Yoon, U. Jeong, Y. Kim, M.H. Cho, D.W. Kim, Biodistribution and toxicity of spherical aluminum oxide nanoparticles, J Appl Toxicol 5 (2015).
[37] J. Scheller, A. Chalaris, D. Schmidt-Arras, S. Rose-John, The pro- and anti-inflammatory properties of the cytokine interleukin-6, Biochimica et Biophysica Acta (BBA) - Molecular Cell Research 1813 (2011) 878-888.
[38] N. Parameswaran, S. Patial, Tumor necrosis factor-alpha signaling in macrophages, Crit Rev Eukaryot Gene Expr 20 (2010) 87-103.
[39] G. Arango Duque, A. Descoteaux, Macrophage cytokines: involvement in immunity and infectious diseases, Front Immunol 5 (2014).
[40] H. Bjorkbacka, K.A. Fitzgerald, F. Huet, X. Li, J.A. Gregory, M.A. Lee, C.M. Ordija, N.E. Dowley, D.T. Golenbock, M.W. Freeman, The induction of macrophage gene expression by LPS predominantly utilizes Myd88-independent signaling cascades, Physiol Genomics 19 (2004) 319-330.
[41] J.J. Gao, V. Diesl, T. Wittmann, D.C. Morrison, J.L. Ryan, S.N. Vogel, M.T. Follettie, Regulation of gene expression in mouse macrophages stimulated with bacterial CpG-DNA and lipopolysaccharide, J Leukoc Biol 72 (2002) 1234-1245.
[42] M.U. Martin, H. Wesche, Summary and comparison of the signaling mechanisms of the Toll/interleukin-1 receptor family, Biochim Biophys Acta 11 (2002) 265-280.
[43] V.V. Sumbayev, I.M. Yasinska, C.P. Garcia, D. Gilliland, G.S. Lall, B.F. Gibbs, D.R. Bonsall, L. Varani, F. Rossi, L. Calzolai, Gold nanoparticles downregulate interleukin-1beta-induced pro-inflammatory responses, Small 9 (2013) 472-477.
[44] C. Roduit, G. Longo, I. Benmessaoud, A. Volterra, B. Saha, G. Dietler, S. Kasas, Stiffness tomography exploration of living and fixed macrophages, J Mol Recognit 25 (2012) 241-246.
[45] G. Ciofani, L. Ricotti, C. Canale, D. D'Alessandro, S. Berrettini, B. Mazzolai, V. Mattoli, Effects of barium titanate nanoparticles on proliferation and differentiation of rat mesenchymal stem cells, Colloids Surf B Biointerfaces 102 (2013) 312-320.

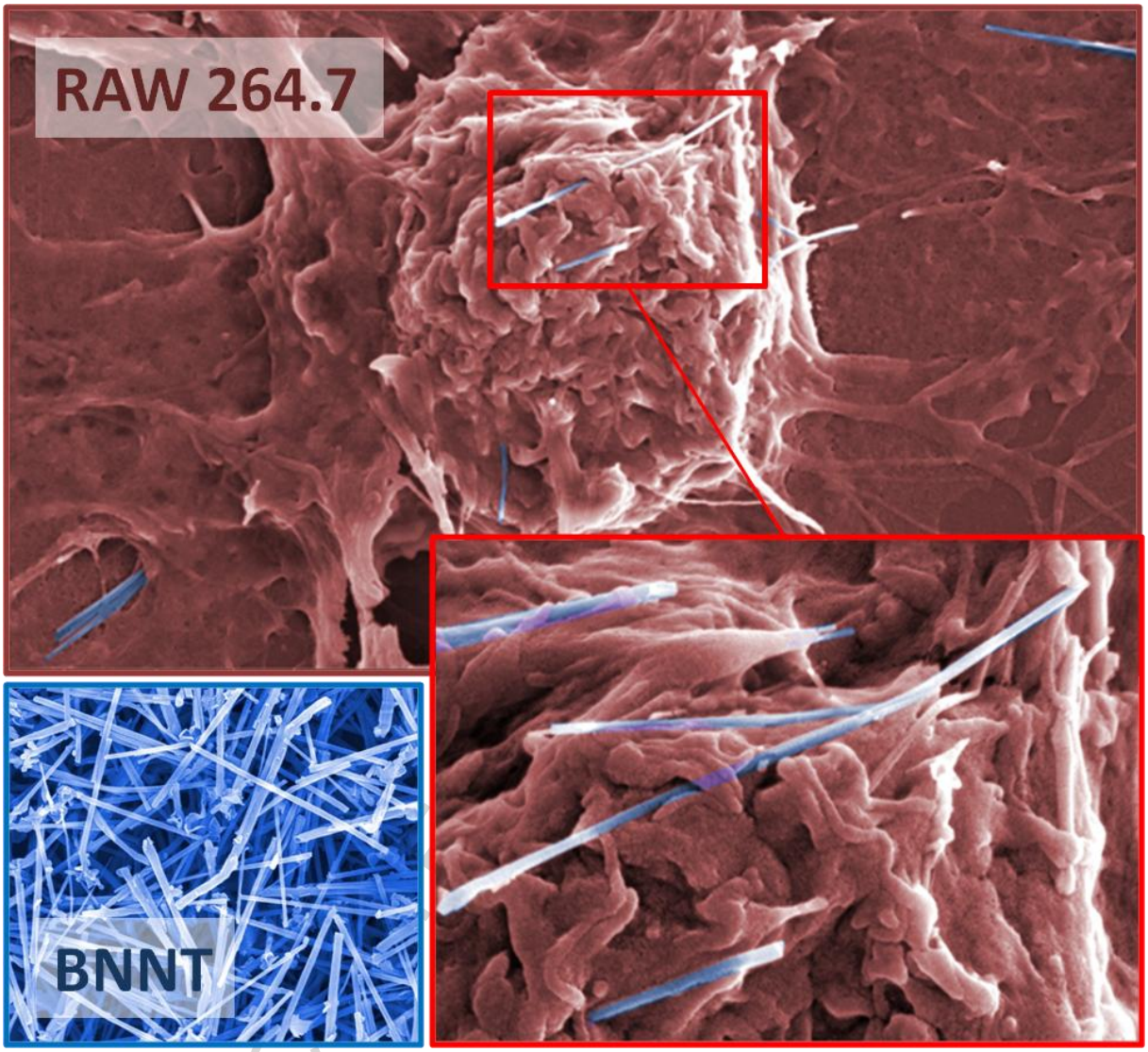

Graphical abstract

Highlights

- Pectin-coated boron nitride nanotubes (BNNTs) have been prepared and tested on RAW 264.7 macrophages.
- This study represents the first investigation of BNNT immune compatibility.
- Collected data indicate absence of acute toxicity and no adverse immune response.
- The suitability of BNNTs for biomedical applications is confirmed.